Induced Charge Oscillations in Dielectric Confined Quasi-2D Systems

Xuanzhao Gao[1, 2, *] and Zecheng Gan[1, 3, †]

[1] *Thrust of Advanced Materials, The Hong Kong University of Science and Technology (Guangzhou), Guangdong, China*
[2] *Department of Physics, The Hong Kong University of Science and Technology, Hong Kong SAR, China*
[3] *Department of Mathematics, The Hong Kong University of Science and Technology, Hong Kong SAR, China*

(Dated: March 7, 2023)

An analytic solution is proposed for the Green's function of dielectric confined quasi-2D systems for which theoretical and simulation investigations are rarely reported due to the difficulty of handling the dielectric mismatch. Based on the solution, we found that under specific confinements, the induced surface charge of an ion shows to be oscillatory, and its *wavelength* is determined by the permittivity and geometry structure of the system. An efficient and accurate algorithm is developed for calculating electrostatic interaction between mobile ions, allowing us to study related physical systems using the molecular dynamics algorithm. The numerical results show that the ions form lattice-like structures triggered solely via the substrate permittivity, owing to the oscillatory property of the induced surface charge.

Introduction.–Quasi-2D systems refer to systems with nano-sized longitudinal thickness in z direction (usually by confinement), bulk-like and modeled as periodic in transverse xy directions [1]. Rich new collective behaviors arise in such systems, to name a few, polyelectrolyte adsorption and structure [2, 3], ion transport and selectivity [4, 5] so that caught much attention. Interestingly, most of these effects concern the permittivity, i.e., the *dielectric confinement effect*. Substrate materials for nanoscale confinement can range from dielectric to metallic, and nowadays, electromagnetic metamaterials, described by permittivities that can take negative values [6, 7] under excitation by electromagnetic waves of specific frequencies. Great efforts have been made to develop negative permittivity materials at very low frequencies [8–10], and recent work has shown that negative static permittivity can be reached in a wide range of materials, such as metals [11], quasi-2D crystals [12], nano-particle [13] and polymeric systems [14].

For electrolytes/polymers near a *single* dielectric substrate, recent calculations have revealed that the dielectric surface effect can considerably deviate the systems from bulk behaviors, such as ion transport [15], polymer brush structure [3] and pattern formation in dipolar films [16], especially when permittivity of the substrate is negative. Unfortunately, the addition of a second dielectric substrate to form dielectric confinement in computer simulations is far from direct-forward: simulation techniques [17–28] have made significant progress over the past decades, but proper treatment of the dielectric confinement effect with satisfactory accuracy and efficiency remains challenging.

In this letter, we develop a method to calculate electrostatic interaction for charged particles in quasi-2D systems under dielectric confinement. By properly renormalization, our method can calculate the electrostatic interaction in meta-material confined systems. We further develop a lattice summation formula for simulating charged particles in such systems, and its spectral convergence allows us to calculate the polarization field efficiently. Applying our method, we show that induced surface charge oscillations arise on substrates under metamaterial confinements. The effect of surface polarization on ionic distributions is further explored through molecular dynamic (MD) simulations of a prototypical charge- and size-symmetric binary mixture of particles described by the primitive model [29], which demonstrate that, the polarization charge on the surface can induce the system to form lattice-like structures and size of the lattice cell can be controlled by tuning the permittivity and thickness of the system.

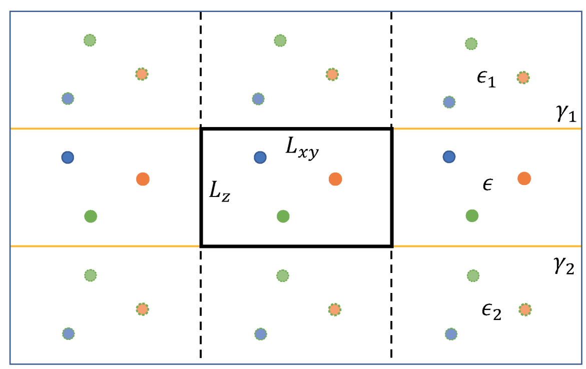

FIG. 1. Schematic depiction of a quasi-2D charged system, the dielectric confinement effect is illustrated from the Image Charge Method (ICM) viewpoint. The middle layer represents the solvent medium with dielectric permittivity ϵ; the upper and lower layers represent the substrate with dielectric permittivity ϵ_1 and ϵ_2, respectively. Colored circles surrounded by solid lines are real charged particles of the doubly-periodic system, while those surrounded by dotted lines are image charges reflected by dielectric interfaces in z.

The model.–The geometry of the dielectric confined quasi-2D systems modeled for simulations is shown in Fig. 1, which is doubly periodic in the transverse direction and finite in the longitudinal direction with edge length of L_x, L_y and L_z. All charged particles are distributed between the dielectric substrates with dielectric permittivity ϵ_1 and ϵ_2, and immersed in solvent with dielectric permittivity ϵ. Based on the ICM, the dimensionless coefficient reflection rate, γ_1 and γ_2 given by $(\epsilon - \epsilon_i)/(\epsilon + \epsilon_i)$, quantify the strength of polarization. Then Green's function of Poisson's equation in such systems can be constructed via a multiple reflection process, resulting in an infinite image charge series, schematically illustrated in Fig. 1. Note that when $|\gamma_1\gamma_2| \leq 1$, the image reflection series is convergent; but when $|\gamma_1\gamma_2| > 1$, it will be *divergent* and thus the reflective ICM approach would fail. Due to this divergence difficulty, current simulation studies in the $|\gamma| \geq 1$ regime is still limited to a single dielectric substrate [16]. Our new approach overcomes this divergence issue via a proper renormalization strategy, which allows us to extensively explore the dielectric confinement effect in all possible γ regimes, especially the less explored scenario of metamaterial substrates with static negative permittivity.

Green's function $G(\boldsymbol{r}, \boldsymbol{s})$ for Poisson's equation of a dielectric confined quasi-2D system is given by

$$-\boldsymbol{\nabla} \cdot [\eta(\boldsymbol{r})\boldsymbol{\nabla} G(\boldsymbol{r}, \boldsymbol{s})] = 4\pi\delta(\boldsymbol{r} - \boldsymbol{s}) \ , \tag{1}$$

where $\boldsymbol{r}$, $\boldsymbol{s}$ are target and source locations under the confined geometry. Importantly, $\eta(\boldsymbol{r}) = \epsilon(\boldsymbol{r})/\epsilon$ characterizes the relative dielectric function which is piecewise constant. Here, $\epsilon(\boldsymbol{r})$ is the material-specific, spatially varying dielectric constant, defined as

$$\epsilon(\boldsymbol{r}) = \begin{cases} \epsilon_1, & z > L_z \\ \epsilon, & 0 \leq z \leq L_z \\ \epsilon_2, & z < 0 \end{cases} \ , \tag{2}$$

as is depicted in Fig. 1. Finally, we have the dielectric interface conditions, i.e., the continuity of $G(\boldsymbol{r}, \boldsymbol{s})$ and $\epsilon(\boldsymbol{r})\partial_z G(\boldsymbol{r}, \boldsymbol{s})$ across $z = 0$ and L_z, and the free-space boundary condition (FBC) as $z \to \pm\infty$. Note that for charges under dielectric confinement, proposing the proper FBC needs careful consideration to make it physically well-defined, which we will clarify later. In the following discussion, we set $\epsilon = 1$ and $\epsilon_1 = \epsilon_2 = \epsilon'$ so that $\gamma_1 = \gamma_2 = \gamma$, by changing ϵ', we vary γ from -10 to 10. Such systems can be achieved via tuning permittivity of the substrates material. For example, the permittivity of VO_2 will reach about -14 at about 350K [11], so that by choosing solvents with permittivity of 11.4 or 17.1 (e.g. organic solvents), the proposed γ can be achieved.

Oscillatory single particle field.–The dielectric confinement effect turns out to be physically attractive even when only one charged particle is present. In Fig. 2 (a), we plot the electric field in x of a cation with valence $\nu = 1$ at (x_0, y_0, τ_0) in a quasi-2D system with thickness of $10\tau_0$, as a function of distance from the cation $\Delta x = x - x_0$, and the confinements are characterized by reflection rate γ. The field is defined

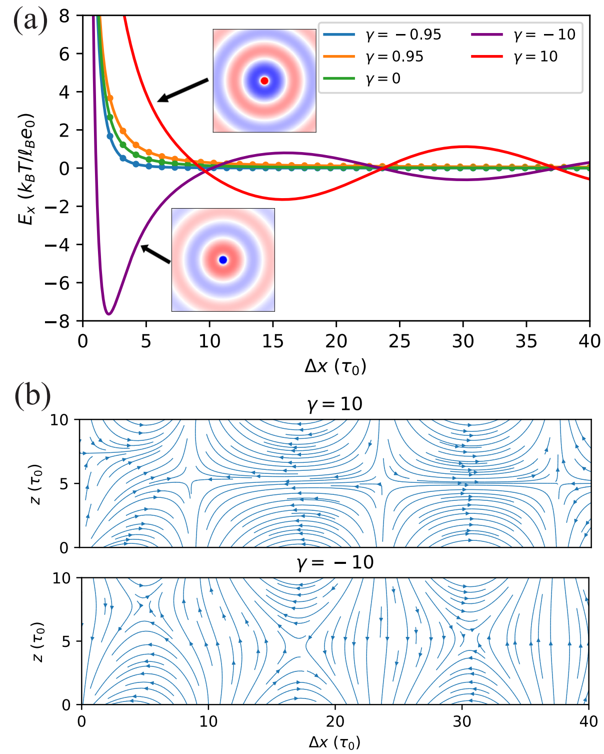

FIG. 2. Electric fields in x by a cation with valence $\nu = 1$ fixed at $(z = \tau_0)$ confined by a pair of dielectric substrates at $z = 0$ and $10\tau_0$ are shown in (a) and the sub-figures represent surface charge density on the lower substrates. For $\gamma = \pm 10$ cases, the corresponding field lines are plotted in (b).

as $-\nu\ell_B\partial_x G(\boldsymbol{r}, \boldsymbol{r_0})$, with $G(\boldsymbol{r}, \boldsymbol{r_0})$ given later in Eq. (10), and the coupling parameter $\ell_B = e^2/(4\pi\epsilon_0\epsilon k_B T)$ is the Bjerrum length of the solvent with the elementary charge e, the vacuum permittivity ϵ_0, the Boltzmann constant k_B, and temperature T. For $|\gamma| < 1$ cases, as shown by blue and orange lines in Fig. 2 (a), the Coulomb effect is enhanced or reduced because of polarization on the surface comparing to $\gamma = 0$ case, respectively. It also shows that our method agrees well with ICM, its results are shown as dots in Fig. 2 (a). However, when $|\gamma| > 1$, the result is highly non-trivial, as shown by purple and red lines. The short-range interaction behave as strongly repulsive or attractive when $\gamma = 10$ or -10, respectively, which can be regarded as an extension of that in $\gamma < 1$ cases. Interestingly, the field did not decay to 0 but shows to be oscillatory in the transverse direction, which is different from previous observations.

Polarization charge on the surface $(z = 0)$ is shown as the sub-figures of Fig. 2 (a) explain the non-trivial behavior of the field, which is defined as

$$\sigma(\boldsymbol{r}) = \lim_{z \to 0^+} \nu\ell_B\epsilon_0 \left(1 - \frac{\epsilon}{\epsilon'}\right) \partial_z G(\boldsymbol{r}, \boldsymbol{r_0}) \ , \tag{3}$$

and the field lines in the xOz plane generated by the surface charge are shown in Fig. 2 (b). These self-consistent results may give an qualitative explain to the non-trivial behavior of the field. At the center, the strong surface charge dominate in both cases as expected, so that even reverse the field. For the long-range field, the surface charge also oscillates along the transverse direction, caused by the intense polarization at the center and enhanced by the bi-surface reflection, generating corresponding fields. The oscillatory field here has a similar structure to that of a surface plasmonic wave but have a different origin, it arise from the reflection by the substrates. It is also shown that for $\gamma > 0$ and $\gamma < 0$ cases, polarize charge and field in z on the opposite substrates are anti-symmetric and symmetric, respectively, which is self-consistent with the definition of γ.

More interestingly, for both cases, the *wavelength* λ of the field, defined as two times the distance between nearby zero points, is only related to resonance frequency of the system, given by

$$k_0 = \frac{\ln \gamma_1\gamma_2}{2L_z} , \tag{4}$$

which will be further discussed below, and via numerical calculation we found they have a simple relation

$$\lambda \cdot k_0 \sim 2\pi . \tag{5}$$

We find that Eq. (5) is highly robust, the relation is irrelevant to $\boldsymbol{r}$, $\boldsymbol{r}_0$, γ or L_z once k_0 is given, as shown in Fig. 3, which means that the effect can be accurately controlled by adjusting k_0.

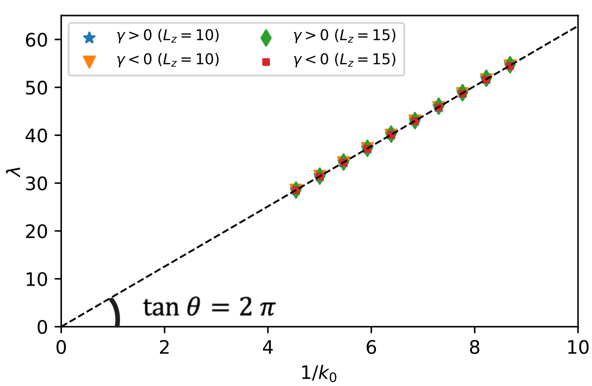

FIG. 3. Numerical results for relation between k_0 and λ. The system parameters, γ and L_z, are changed to tune k_0. For each point in the figure, we calculated the interaction between a pair of particles with randomly generated position in z as a function of $\Delta\rho$. Then the average distance between zero points of E_x is taken as $\lambda/2$.

Eq. (1) can be solved directly because of the special geometry. To start, one applies plane wave expansion on both sides of the equation so that the Green's function can be expressed as

$$\begin{aligned} G(\boldsymbol{r},\boldsymbol{s}) &= -\frac{1}{\pi}\iint_{\mathbb{R}^2} g(k,z,z_s)e^{-i\boldsymbol{k}\cdot\Delta\boldsymbol{\rho}}\mathrm{d}k_x\mathrm{d}k_y \\ &= -\int_0^{+\infty} 2g(k,z,z_s)J_0(k\Delta\rho)k\mathrm{d}k , \end{aligned} \tag{6}$$

where $\boldsymbol{k} = (k_x, k_y)$, $\Delta\boldsymbol{\rho} = (x - x_s, y - y_s)$. When $k > 0$, $g(k, z, z_s)$ is given as

$$g(k,z,z_s) = \frac{1}{2k}\frac{1}{\gamma_1\gamma_2\exp(-2kL_z)-1}\sum_{i=1}^{4}\Gamma_l \mathrm{e}^{-ka_l} , \tag{7}$$

where $\Gamma_l = [1,\ \gamma_1,\ \gamma_2,\ \gamma_1\gamma_2]$ and $a_l = [|z - z_s|,\ z + z_s,\ 2L_z - (z+z_s),\ 2L_z - |z - z_s|] \in [0, 2L_z]$. When $k = 0$, the solution is given by

$$g(k=0,z,z_s) = -\frac{|z-z_s|}{2}. \tag{8}$$

Physically, Eq. (8) implies that for $k = 0$, confined source charge acts as a uniformly charged plate.

Although $g(k, z, z_s)$ is solved analytically, integral of Eq. (7) is divergent for $\gamma_1\gamma_2 > 1$ cases, because $g(k, z, z_s)$ divergent at k_0, which has been given in Eq. (4), so that the integral need to be renormalized. Notice that when $k \to k_0$, the divergent factor has the property

$$\frac{1}{\gamma_1\gamma_2\exp(-2kL_z)-1} \to \frac{1}{2L_z(k_0-k)} , \tag{9}$$

so that k_0 is a first-order pole and the Cauchy principal value exists. Then Eq. (6) for $\gamma_1\gamma_2 > 1$ cases is given by

$$G(\boldsymbol{r},\boldsymbol{s}) = -\text{p.v.}\left[\int_0^{+\infty} 2g(k,z,z_s)J_0(k\Delta\rho)k\mathrm{d}k\right] , \tag{10}$$

which can be calculated numerically. Eq. (10) may give an explanation to the relation in Eq. (5). All terms in Eq. (10) can be simplified as

$$I_o = \int_0^{\infty}\frac{J_0(k\Delta\rho)\mathrm{e}^{-ka}}{\exp(2L_z(k_0-k))-1}\mathrm{d}k , \tag{11}$$

where $\Delta\rho$, k_0 and a are all positive constants. We find that the oscillation in I_o can be further transformed as

$$I_o = \frac{e^{-k_0 a}}{2L_z}\int_0^{\infty}\frac{J_0(k')}{k_0-k'}\mathrm{d}k' + f(k_0,\Delta\rho,a) \tag{12}$$

where $k' = k\Delta\rho$, and $f(k_0, \Delta\rho, a)$ is a non-oscillatory analytic function which contributes less to I_o (details are shown in SI). The first integral can be regarded as a function of $k_0\Delta\rho$, label as $I_m(k_0\Delta\rho)$, which is unrelated to other parameters, so that is general for any given parameters. Numerical result shows that distance between zero points of $I_m(k_0\Delta\rho)$ converge rapidly to π, which leads to the near periodic property of the field and the relation given by Eq. (5).

Collective phases.–To study how the oscillation can influence the phase behaviors of quasi-2D charged systems, we further developed a molecular dynamics (MD) algorithm by inducing idea of Ewald splitting, details are shown in SI. We examine a prototypical quasi-2D charged system, a binary mixture of charged particles described by the primitive model. The system contains $N/2$ cations and $N/2$ anions, each particle with the same diameter τ_0 and valence ± 1, and is thus overall charge neutral. Assume i-th particle is located at $\boldsymbol{r_i}$ and carries charge q_i, the Hamiltonian of the system reads

$$\mathcal{H} = \frac{1}{2}\sum_{i,j=1}^{N}{}' q_i q_j \ell_B G(\boldsymbol{r}_i, \boldsymbol{r}_j) + U_{\mathrm{LJ}} , \tag{13}$$

where $\sum_{i,j}{}'$ indicates that when $i = j$, $G(\boldsymbol{r})$ is for the self-interaction, and U_{LJ} is the shift-truncated Lennard-Jones (LJ) potential energy modeling the excluded-volume interactions. The present model discards other interactions that may be important in experimental realizations but also offers the advantage of isolating the dielectric confinement effect. Systems with similar setups have been investigated recently in Refs. [24, 26, 27].

In all the Molecular Dynamics (MD) simulations performed, we fix box size in xy as $180\tau_0 \times 180\tau_0$ so that the boundary effect can be ignored at the central area, then we tune L_z and γ to change k_0. The Bjerrum length for the solvent medium is set to be $\ell_{\mathrm{B}} = 3.5\tau_0$. Temporal integration is performed via the Velocity-Verlet algorithm provided by LAMMPS [30], and temperature is controlled via Anderson thermostat with stochastic collision frequency $\omega = 0.1$.

Interestingly, we found the ions are induced to form clusters, and the clusters order periodically in both $\gamma > 1$ and $\gamma < -1$ cases near the substrates in the transverse direction, as shown in Fig. 4 (a); in the vertical direction, the ions are distributed near the substrates, and are paired with another cluster on the opposite side anti-symmetrically and symmetrically, respectively. The structures of the clusters are also different, when $\gamma < -1$, the ions are closely packed, and when $\gamma > 1$, they form ion liquid, because the interactions between charges are attractive and repulsive, respectively, as shown in Fig. 2 (a). We attribute the lattice formation process to the periodical oscillation of field as shown in Fig. 2 (a), which allows all charges to induce the same kind of surface charge to another cell so that forms lattice-like potential well and confine the charges within.

The idea can be further proved by the relation shown in Fig. 4 (b), which shows that the lattice constant of our system is also linear to k_0^{-1}, so that is proportional to the wavelength which can be tuned by the structure of the quasi-2D system. It is also shown that the slopes are slightly different, 1.2π and 1.4π for $\gamma < 0$ cases and $\gamma > 0$ cases, respectively, proportional to distance between the nearest neighbors, which are slightly smaller or larger than the second zeros point of surface charge excited by a point charge near the surface. In both cases, for each clusters, its nearest neighbors induce surface with different sign below it and thus form the potential well. Under the combined action of all clusters, interaction between ions and the surface charge dominate and the special checkerboard structure is built.

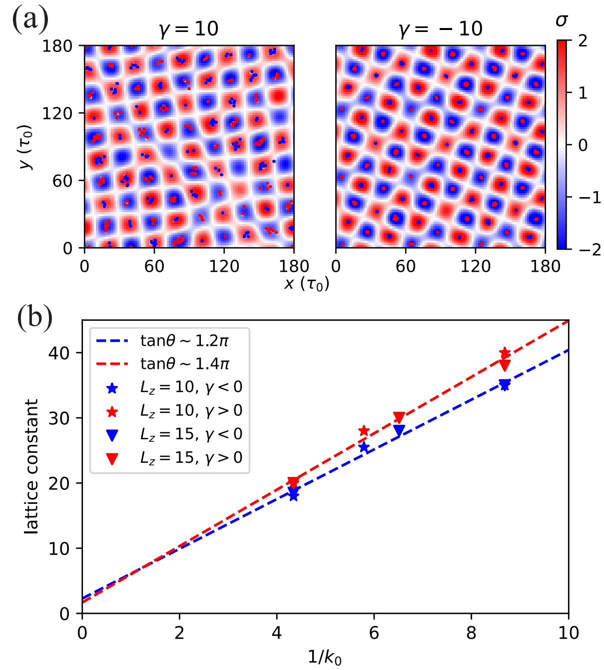

FIG. 4. Charge distribution near the lower substrate and surface charge density for $\gamma = \pm 10$, $L_z = 10$ cases are shown in (a), where red and blue are for the positive and negative charge, respectively. The relation between the lattice constant and system parameters is shown in (b), where the dots are the sampling points and the dashed lines are the fitting result.

Conclusions.–In summary, by a properly renormalizing solution of Poisson's equation in a dielectric confined quasi-2D system, we find that polarizable substrates with negative permittivity can turn field of a point charge into an oscillatory one. Then using a newly developed lattice summation method that permits simulations of such systems, we found that lattice formation may happen because of the oscillatory field, and the system can be controlled by adjusting the resonance frequency k_0. Our approach also provides a powerful tool for efficient and accurate simulation for a broad range of quasi-2D systems, with wide applications in future nanotechnology. The future plan includes further explore phase behavior of the dielectric confined quasi-2D charged systems and an open source implementation in LAMMPS [30].

Z. Gan acknowledges financial support from the National Science Foundation under Award No. CBET-1804940 and DMR-1420073. Z. Gan also wish to thank Aleksandar Donev and Leslie Greengard for helpful discussions on the physics and algorithms for quasi-2D charged systems. X. Gao wish to thank Hongchao Li and Mingzhe Li for fruitful discussions.

* xz.gao@connect.ust.hk
† Corresponding author; zechenggan@ust.hk

[1] M. Mazars, Long ranged interactions in computer simulations and for quasi-2D systems, Phys. Rep. **500**, 43 (2011).
[2] R. Messina, Effect of image forces on polyelectrolyte adsorption at a charged surface, Phys. Rev. E **70**, 051802 (2004).
[3] J. Yuan, H. S. Antila, and E. Luijten, Structure of polyelectrolyte brushes on polarizable substrates, Macromolecules **53**, 2983 (2020).
[4] M. Nishizawa, V. P. Menon, and C. R. Martin, Metal Nanotubule Membranes with Electrochemically Switchable Ion-Transport Selectivity, Science **268**, 700 (1995).
[5] J. Cervera, B. Schiedt, R. Neumann, *et al.*, Ionic conduction, rectification, and selectivity in single conical nanopores, J. Chem. Phys. **124**, 104706 (2006).
[6] V. G. Veselago, Electrodynamics of substances with simultaneously negative ϵ and ν, Usp Fiziol Nauk **92**, 517 (1967).
[7] D. R. Smith, J. B. Pendry, and M. C. Wiltshire, Metamaterials and Negative Refractive Index, Science **305**, 788 (2004).
[8] C. Cheng, R. Fan, Z. Wang, Q. Shao, X. Guo, P. Xie, Y. Yin, Y. Zhang, L. An, Y. Lei, *et al.*, Tunable and weakly negative permittivity in carbon/silicon nitride composites with different carbonizing temperatures, Carbon **125**, 103 (2017).
[9] P. Xie, Z. Shi, M. Feng, K. Sun, Y. Liu, K. Yan, C. Liu, T. A. Moussa, M. Huang, S. Meng, *et al.*, Recent advances in radio-frequency negative dielectric metamaterials by designing heterogeneous composites, Advanced Composites and Hybrid Materials **5**, 679 (2022).
[10] X. Xu, Q. Fu, H. Gu, Y. Guo, H. Zhou, J. Zhang, D. Pan, S. Wu, M. Dong, and Z. Guo, Polyaniline crystalline nanostructures dependent negative permittivity metamaterials, Polymer **188**, 122129 (2020).
[11] J. K. Kana, G. Vignaud, A. Gibaud, and M. Maaza, Thermally driven sign switch of static dielectric constant of VO_2 thin film, Opt. Mater. **54**, 165 (2016).
[12] V. U. Nazarov, Negative static permittivity and violation of Kramers-Kronig relations in quasi-two-dimensional crystals, Phys. Rev. B **92**, 161402 (2015).
[13] J. Shulman, S. Tsui, F. Chen, Y. Xue, and C. Chu, Plasmalike negative capacitance in nanocolloids, Appl. Phys. Lett. **90**, 032902 (2007).
[14] H. Yan, C. Zhao, K. Wang, L. Deng, M. Ma, and G. Xu, Negative dielectric constant manifested by static electricity, Appl. Phys. Lett. **102**, 062904 (2013).
[15] H. S. Antila and E. Luijten, Dielectric Modulation of Ion Transport near Interfaces, Phys. Rev. Lett. **120**, 135501 (2018).
[16] Z. Wang and E. Luijten, Dielectric Modulation of Two-Dimensional Dipolar Materials, Phys. Rev. Lett. **123**, 096101 (2019).
[17] A. Arnold, J. de Joannis, and C. Holm, Electrostatics in periodic slab geometries. I, J. Chem. Phys. **117**, 2496 (2002).
[18] J. de Joannis, A. Arnold, and C. Holm, Electrostatics in periodic slab geometries. II, J. Chem. Phys. **117**, 2503 (2002).
[19] S. Tyagi, A. Arnold, and C. Holm, ICMMM2D: An accurate method to include planar dielectric interfaces via image charge summation, J. Chem. Phys. **127**, 154723 (2007).
[20] A. Fernández-Domínguez, S. Maier, and J. Pendry, Collection and Concentration of Light by Touching Spheres: A Transformation Optics Approach, Phys. Rev. Lett. **105**, 266807 (2010).
[21] V. Jadhao, F. J. Solis, and M. O. De La Cruz, Simulation of Charged Systems in Heterogeneous Dielectric Media via a True Energy Functional, Phys. Rev. Lett. **109**, 223905 (2012).
[22] J. W. Zwanikken and M. Olvera de La Cruz, Tunable soft structure in charged fluids confined by dielectric interfaces, Proc. Natl. Acad. Sci. U.S.A. **110**, 5301 (2013).
[23] F. Fahrenberger and C. Holm, Computing the Coulomb interaction in inhomogeneous dielectric media via a local electrostatics lattice algorithm, Phys. Rev. E **90**, 063304 (2014).
[24] A. P. Dos Santos, M. Girotto, and Y. Levin, Simulations of Coulomb systems confined by polarizable surfaces using periodic Green functions, J. Chem. Phys. **147**, 184105 (2017).
[25] S. Yu and H. Ammari, Plasmonic Interaction between Nanospheres, SIAM Rev. **60**, 356 (2018).
[26] J. Liang, J. Yuan, E. Luijten, and Z. Xu, Harmonic surface mapping algorithm for molecular dynamics simulations of particle systems with planar dielectric interfaces, J. Chem. Phys. **152**, 134109 (2020).
[27] J. Yuan, H. S. Antila, and E. Luijten, Particle–Particle Particle–Mesh algorithm for electrolytes between charged dielectric interfaces, J. Chem. Phys. **154**, 094115 (2021).
[28] O. Maxian, R. P. Peláez, L. Greengard, and A. Donev, A fast spectral method for electrostatics in doubly periodic slit channels, J. Chem. Phys. **154**, 204107 (2021).
[29] W. G. McMillan Jr and J. E. Mayer, The Statistical Thermodynamics of Multicomponent Systems, J. Chem. Phys. **13**, 276 (1945).
[30] A. P. Thompson, H. M. Aktulga, R. Berger, *et al.*, LAMMPS - a flexible simulation tool for particle-based materials modeling at the atomic, meso, and continuum scales, Comp. Phys. Comm. **271**, 108171 (2022).